



# Weathering of Chlorite Illite Deposits in the Hyperarid Qaidam Basin: Implications to Post-Depositional Alteration on Martian Clay Minerals

Yu Sun<sup>1\*</sup>, Yiliang Li<sup>2,3</sup>, Chaoqun Zhang<sup>1</sup>, Xiaorong Qin<sup>4,5</sup>, Jianxun Shen<sup>1</sup>, Hongping He<sup>4,5</sup> and Yongxin Pan<sup>1,5</sup>

<sup>1</sup>Key Laboratory of Earth and Planetary Physics, Institute of Geology and Geophysics, Chinese Academy of Sciences (CAS), Beijing, China, <sup>2</sup>Department of Earth Sciences, University of Hong Kong, Pokfulam, Hong Kong SAR, China, <sup>3</sup>CAS Center for Excellence in Comparative Planetology, Hefei, China, <sup>4</sup>CAS Key Laboratory of Mineralogy and Metallogeny/Guangdong Provincial Key Laboratory of Mineral Physics and Materials, Guangzhou Institute of Geochemistry, Chinese Academy of Sciences, Guangzhou, China, <sup>5</sup>University of Chinese Academy of Sciences, Beijing, China

## OPEN ACCESS

### Edited by:

Alberto Fairén,  
Center for Astrobiology (CSIC), Spain

### Reviewed by:

Elizabeth Rampe,  
National Aeronautics and Space  
Administration (NASA), United States  
Thomas Bristow,  
National Aeronautics and Space  
Administration (NASA), United States

### \*Correspondence:

Yu Sun  
sunyu@mail.iggcas.ac.cn

### Specialty section:

This article was submitted to  
Astrobiology,  
a section of the journal  
Frontiers in Astronomy and Space  
Sciences

Received: 14 February 2022

Accepted: 25 April 2022

Published: 23 May 2022

### Citation:

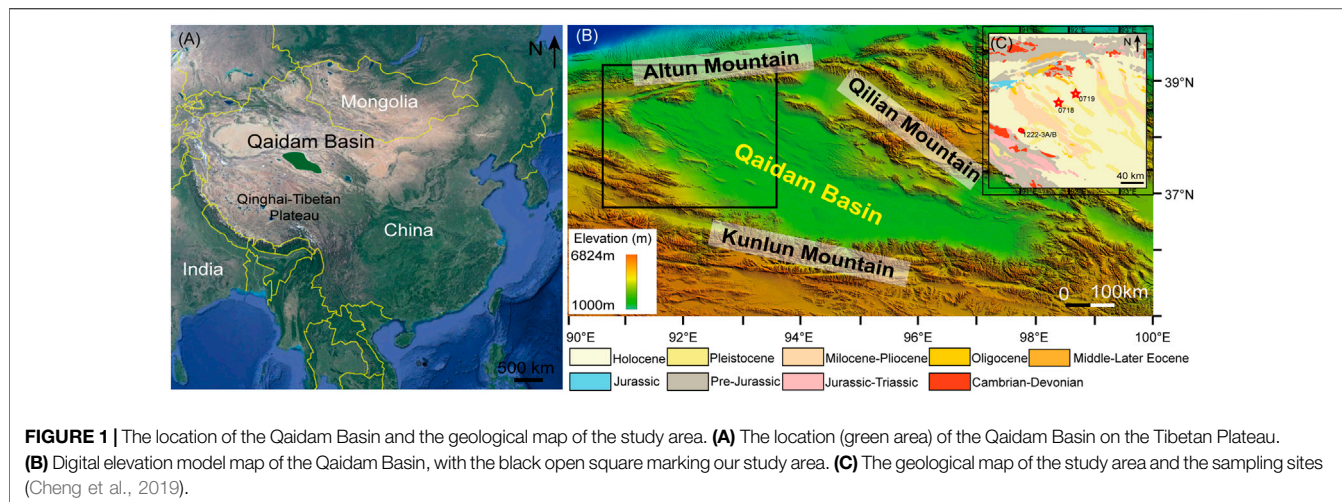
Sun Y, Li Y, Zhang C, Qin X, Shen J, He H and Pan Y (2022) Weathering of Chlorite Illite Deposits in the Hyperarid Qaidam Basin: Implications to Post-Depositional Alteration on Martian Clay Minerals. *Front. Astron. Space Sci.* 9:875547. doi: 10.3389/fspas.2022.875547

Chlorite is the second-most common class of clay minerals on the Martian surface and has been found to coexist with illite in some regions. Although previous studies have paid much attention to the formation of this assemblage, the post-depositional evolution cannot be neglected because the aqueous activities may alter the mineral assemblage and distribution. Here, we report on the post-depositional weathering of lacustrine-fluvial deposits collected from yardangs and dune-covering lake beds in the western Qaidam Basin, one of the largest and highest terrestrial Mars analogs. Mineralogical analysis shows that Fe-clinocllore and illite are the main clay components deposited as detrital particles. Electron microscopic observations of small rusty concretions from yardang deposits revealed that iron was released from clinocllore and formed ferrihydrite in fractures. We suggest that the activities of ephemeral waters after the deposition provide the major source of water that influences the migration of Fe in a long-lasting hyperarid climate. A similar iron-releasing mechanism could have occurred in Nili Fossae on Mars because multiple aqueous activities have shaped the terrains where chlorite illite deposits were identified by orbital near-infrared reflectance spectroscopy. Thus, reconstruction of the aqueous history of ancient Mars from surface minerals requires consideration of post-depositional processes, since groundwater/meteoritic water may continuously interact with clay mineral-bearing deposits on Mars after their formation.

**Keywords:** chlorite, illite, Qaidam Basin, Mars, weathering

## INTRODUCTION

The global distribution of clay minerals on the Martian surface demonstrates the liquid water activity on ancient Mars (Poulet et al., 2005; Bibring et al., 2006; Bishop, 2018). Among clay members of the phyllosilicate group identified from the orbital datasets of Mars, the content of chlorite is higher than that of all the other members with the exception of smectite (Ehlmann et al., 2011a; Ehlmann et al., 2011b). Similar to smectite, Martian chlorite is also rich in Fe and Mg (Ehlmann et al., 2011a). Chlorite is a hydrous phyllosilicate-type mineral with an interlayer hydroxide octahedral sheet between two structural layered units, forming a special 2:1:1 layered structure (Kohut and Warren,



2002). According to different enriched metallic elements that occupy the octahedral sheet, chlorite can be divided into four subtypes—clinochlore ( $Mg^{2+}$ -rich), chamosite ( $Fe^{2+}$ -rich), nimitite ( $Ni^{2+}$ -rich), and pennantite ( $Mn^{2+}$ -rich) (Kohut and Warren, 2002). However, due to element substitutions, clinochlore can also be rich in  $Fe^{2+}$  (Smyth et al., 1997), as  $Fe^{2+}$  and  $Mg^{2+}$  are the dominant divalent cations in the octahedral sheets (Aja et al., 2015). Chlorite can be formed through the diagenesis of smectite, hydrothermal alteration, and metamorphism, and it could be further weathered to vermiculite in warm and wet terrestrial surface conditions (Ehlmann et al., 2011a).

On Mars, chlorite has been identified mainly by visible/near-infrared (VNIR) spectra obtained by the Compact Reconnaissance Imaging Spectrometer for Mars (CRISM) onboard the Mars Reconnaissance Orbiter (MRO) and Observatoire pour la Minéralogie, l'Eau, les Glaces et l'Activité (OMEGA) onboard the Mars Express orbiter (Poulet et al., 2005; Ehlmann et al., 2011b). In some cases, chlorite coexists with prehnite near craters, indicating the presence of hydrothermal activity driven by impacts (Ehlmann et al., 2009; Ehlmann et al., 2011a). Alteration mineral assemblages are also discovered in central peaks of craters where chlorite is associated with Fe, Mg-smectite, analcime, and hydrated silica (Milliken et al., 2008; Ehlmann et al., 2009).

Another phyllosilicate, illite, is structurally a 2:1 type of phyllosilicate composed of two tetrahedral sheets sandwiched by one octahedral sheet (T-O-T) (Ehlmann et al., 2009). Although illite is indistinguishable from muscovite in CRISM and OMEGA data (Ehlmann et al., 2009), it may coexist with chlorite as the main weathering-derived clay member on Mars. In the region of Nili Fossae, both chlorite and illite are identified based on the CRISM data (Ehlmann et al., 2009). Considering the mineral composition and the aqueous history of this region, (Ehlmann et al., 2009), suggest that the fluvial activity and sapping channel formation could affect the distribution of these minerals. Therefore, the post-depositional effects caused by later water activity are significant for understanding the aqueous history and the mineral transformation during the long evolution of the Martian paleoclimate.

The Qaidam Basin, located on the northern edge of the Tibetan Plateau (Figure 1A), has formed a vast area of playas and eolian landscapes due to the blocking of moisture by surrounding mountain ranges of >5,000-m altitude (Figure 1B) and the resultant prolonged hyperarid climate (Han et al., 2014). After a similar climate transition from wet to dry, the surface landforms and changing surface environments of the Qaidam Basin are analogous to those proposed for ancient Mars (Kong et al., 2018). The basin has maintained high aridity, with a current evaporation rate of 2,590 mm/yr and a precipitation rate of <20 mm/yr (Kong et al., 2018). The average annual surface temperature of the western Qaidam basin is 3.5°C, with the maximum monthly average air temperature of 16°C in July and the minimum monthly average air temperature of -10.7°C in January (Kong et al., 2018). Thus, numerous previous studies exemplify Qaidam as one of the highest environmental Mars analogs (Xiao et al., 2016; Anglés and Li, 2017; Sun et al., 2019; Sun et al., 2021). Here, we report alteration of chlorite illite-bearing deposits in two areas: weathered yardang (basin center) and dune-covered (basin margin) deposits in the western Qaidam Basin. By evaluating the post-depositional effects on these deposits in a dry and cold Mars analogous environment, this study seeks to provide constraints on the evolution of widespread iron-bearing phyllosilicate on Mars.

## SAMPLES AND METHODS

Four samples of this study were collected in lacustrine-fluvial deposits from western Qaidam Basin: the yardang samples (named 0718 and 0719) at  $N38^{\circ}2'6.4''$ ,  $E91^{\circ}51'8.39''$ , and  $N38^{\circ}12'40.716''$ ,  $E92^{\circ}4'15.276''$ , respectively; the dune-covered samples (named 1222-3A and 3B) at  $N37^{\circ}50'58.6''$ ,  $E91^{\circ}4'6.5''$  (Figure 1C). These samples were collected in the vast area of the Holocene playa (Figure 1C), representing the last massive liquid water event (Han et al., 2014) that has been shaping the depocenter of the western Qaidam Basin ever since. After the disappearance of the northwestern center of the mega-lake, the

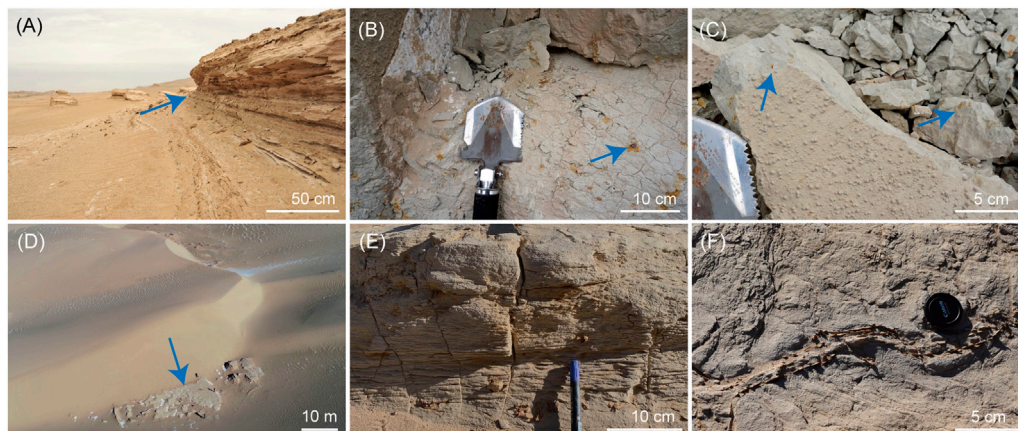


**FIGURE 2** | Sampling sites and samples from the western Qaidam Basin. **(A)** Deposits are exposed on the side of a yardang (blue arrow). **(B,C)** Yardang samples (0718 and 0719) with rusty concretions (blue arrows). **(D)** Deposits (yellow arrow) are covered by sand dunes from the view of a drone. **(E,F)** Dune-covering samples (1222-3A and 3B).

surface is featured by strong wind-sculpted yardang fields (Xiao et al., 2016). Thin layers of carbonate ooids were found actively formed 38,000 years ago near the yardang sampling area (Sun et al., 2019), indicating that these deposits should be exposed later than this period. Otherwise, evaporites would have cemented the deposits. In the western Qaidam Basin, yardang fields display various morphologies and sizes due to winds with different strengths and directions. The yardang fields now cover an area of  $3.88 \times 10^4 \text{ km}^2$  in the Qaidam Basin (Xiao et al., 2016). The two yardang samples were collected on the lower side of the weathered yardangs (Figures 1C, 2A). Samples displayed grey surfaces with rusty small concretions (Figures 2B,C). Sand dunes in the desert, however, have only developed in particular zones in the basin. The dune-covered samples were collected on a fluvial fan of Kunlun Mountain, which is partially covered by a series of barchan dunes (Figures 1C, 2D). These deposits were layered and loose (Figure 2E). Iron-bearing veins exist in these deposits (Figure 2F). Two samples were collected with clean tools from the same site but in different layers and sealed with parafilm tapes to prevent exposure to air moisture during transport to the laboratory.

In addition to the four sediment samples, we collected two purified clay minerals (see **Supplementary Figure S1** for more component information), clinocllore (from Liaoning, China) and illite (from Zhejiang, China), as positive controls in spectral measurements.

The mineral compositions of these samples were determined using a Rigaku MiniFlex-400 X-ray diffractometer (XRD) at the Guangzhou Institute of Geochemistry, Chinese Academy of Sciences (CAS). The diffractometer is equipped with a Hybrid pixel array detector, a Cu source, and a Ni filter. Prior to bulk XRD measurements, samples were ground into fine powder ( $70 \mu\text{m}$ ) using agate mortar. The samples were loaded into rectangular Al holders and tableted for measurements. Data were collected between  $3^\circ$  and  $70^\circ$  with a step size of 0.01 and a dwell time of 1 s in each step. To identify the composition of the rusty parts from these deposits, the rusty concretions were

separated with clean tweezers based on different colors and ground for further XRD measurements.

Spectroscopic analysis was conducted on a Malvern Panalytical TerraSpec 4 Hi-Res spectrometer at the Institute of Geology and Geophysics (IGG), CAS. Before the spectroscopic analysis, samples were oven-dried at  $80^\circ\text{C}$  overnight and separated into bulk clay and rusty parts with tweezers, followed by mild grinding into fine powder. Microstructure and morphology of small particles were recorded using an FEI Apreo S scanning electron microscope (SEM) equipped with a Bruker XFlash 60 energy dispersive spectrometer (EDS) detector and a JEOL JEM-2100 transmission electron microscope (TEM) at IGGCAS. To obtain the natural morphology of the minerals, we use small tweezers to pick out the rusty parts and fix them on the conductive adhesive for direct SEM observation. The samples for TEM observation were ground with an agate mortar for 5 min, dispersed in alcohol, and dropped on the copper grid for analysis.

The rusty concretions were separated from the samples and were ground into fine powder for  $^{57}\text{Fe}$  Mössbauer spectroscopy measurements at room temperature in the transmission mode operating in constant acceleration mode using a Silver Double Limited WSS-10 spectrometer. The Mössbauer source was a  $^{57}\text{Co}$  in the Rh matrix. The velocity drive transducer was operated in a triangular waveform mode over energy ranges of  $\pm 15 \text{ mm/s}$ . The spectroscopic center was calibrated using an  $\alpha\text{-Fe}$  foil. The spectrum was analyzed with the Mosswin 4.0 program. Subspectra attributed to different phases were determined based on their hyperfine parameters [i.e., isomer (IS), quadrupole splitting (QS), and linewidths].

## RESULTS

As shown by the XRD patterns, the mineral components of these deposits were quartz ( $d_{(101)} = 3.34 \text{ \AA}$ ), albite ( $d_{(002)} = 3.18 \text{ \AA}$ ), minor carbonate ( $d_{(104)} = 3.03 \text{ \AA}$ ), and clay minerals identified as Fe-clinocllore and illite in accordance with their main d values

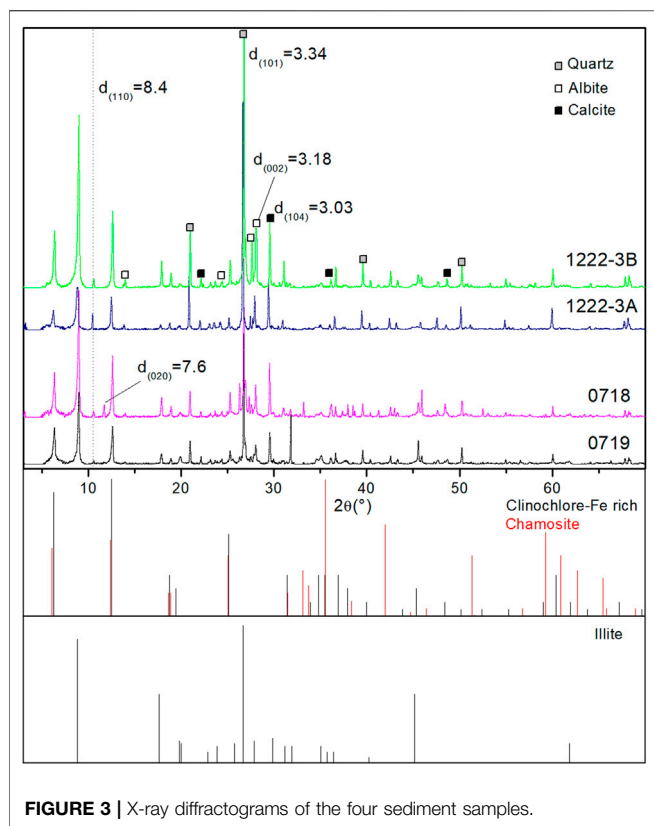


**FIGURE 3** | X-ray diffractograms of the four sediment samples.

( $d_{(001)} = 13.90 \text{ \AA}$  and  $d_{(002)} = 9.90 \text{ \AA}$ ) and the overall pattern features (**Figure 3**). The yardang samples contained minor gypsum ( $d_{(020)} = 7.6 \text{ \AA}$ ), reflecting the evaporation of liquid water in the basin center. The dune-covered deposits displayed characteristic XRD peaks of amphibole ( $d_{(110)} = 8.4 \text{ \AA}$ ) (**Figure 3**), implying that the debris from nearby mountains was only partially weathered.

The XRD patterns of the rusty parts (named 0718-Fe and 0719-Fe) display the same features as the bulk samples (**Figure 4**), indicating no new well-crystallized phase was formed. The intensity ratio of  $d_{(001)}/d_{(003)}$  in XRD patterns was used to determine the Fe content in clinoclchlore (Ryan and Reynolds, 1997). The ratios are 8.84, 4.6 for 0719-Bulk and 0719-Fe; 4.4, 4.2 for 0718-Bulk and 0718-Fe. The decrease of the  $d_{(001)}/d_{(003)}$  ratio indicated that Fe migrated from clinoclchlore to the rusty parts.

SEM micrographs of the bulk samples showed poor morphology of these clay minerals with grain sizes  $< 2 \mu\text{m}$  (**Figures 5A–C**), indicating a debris origin (Wilson, 1999). Halite was observed in the yardang-type samples (**Figure 5B**). In the rusty parts, nanoparticles are distributed on the surface of the clay grains (**Figure 5D**). Backscattered electron imaging associated with the elemental mapping of the same area illustrated that these materials were Fe-enriched (**Figures 5E,F**) but Mg, Al, Si-depleted compared to the surrounding clay grains (**Figures 5G–I**). EDS results confirmed that clinoclchlore in these samples was enriched with Fe, and the content of Fe in the clay mineral was decreased near the Fe enriched area (see **Supplementary Table S1**).

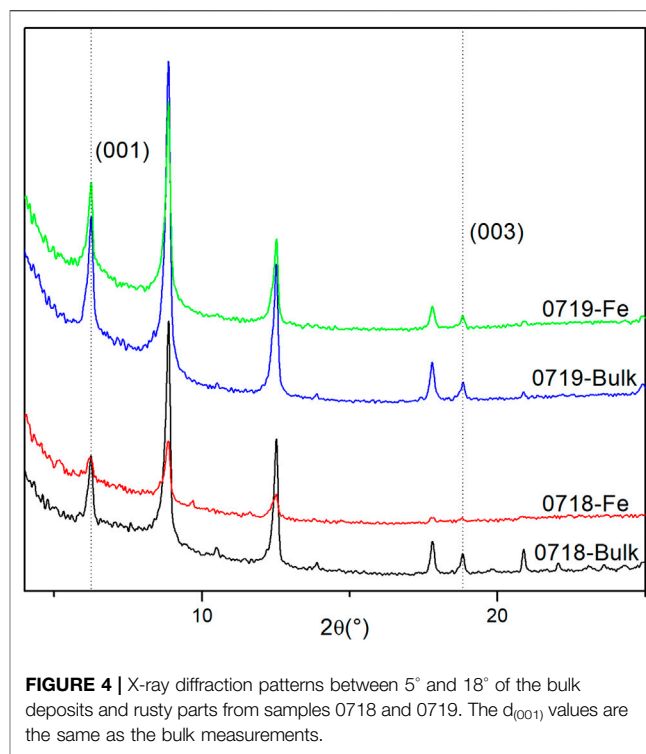


**FIGURE 4** | X-ray diffraction patterns between  $5^\circ$  and  $18^\circ$  of the bulk deposits and rusty parts from samples 0718 and 0719. The  $d_{(001)}$  values are the same as the bulk measurements.

Under TEM (**Figure 6A**), nanoparticles were intimately mixed with clinoclchlore. The magnified image of these minerals again displayed nanophase aggregates with a diameter of  $< 5 \text{ nm}$  (**Figure 6B**). The high-resolution TEM image revealed that the d-spacing of the nanoparticle was  $2.5 \text{ \AA}$  (**Figure 6B**), which corresponded to the 110 panels of ferrihydrite or nanohematite (Jiang et al., 2018).

Mössbauer spectroscopy of the rusty parts provided further identification of the Fe-bearing materials. The spectrum was fitted with two subspectra (**Figure 7**). The doublet with IS, QS values of 1.12 mm/s, and 2.73 mm/s (green) corresponded to the  $\text{Fe}^{2+}$  in the octahedron of chlorite (Pollak and Stevens, 1986). Another doublet with IS, QS values of 0.37 mm/s, 0.61 mm/s (pink) indicated that the octahedral sites of  $\text{Fe}^{3+}$  were relatively disordered, which should be attributed to ferrihydrite as additionally supported by the TEM observations (Murad, 1996).

The NIR spectra of these Qaidam samples displayed combinative features of both clinoclchlore and illite (**Figure 8**). The -OH overtone at  $1.414 \mu\text{m}$  was much weaker than the pure clinoclchlore and illite. The H-O-H combination band at  $1.931 \mu\text{m}$  should be attributed to the coupling of the signals from both clinoclchlore and illite, which moved to a higher wavelength indicative of the increasing content of illite (**Figure 8**). The  $2.211 \mu\text{m}$  absorption was due to the Al-OH in illite (Ehlmann et al., 2009), while the  $\sim 2.347 \mu\text{m}$  absorption was a combination of M-OH (M could be Fe, Mg, or the mix of these cations) in clinoclchlore and illite (Bishop et al., 2008). The CRISM data reported by (Ehlmann et al., 2009) demonstrated a similar NIR pattern with 1.4, 1.9, 2.2, and  $\sim 2.3 \mu\text{m}$  absorptions as compared to the Qaidam samples in this study, indicating the deposition of the chlorite illite assemblage in the Nili Fossae region on Mars.

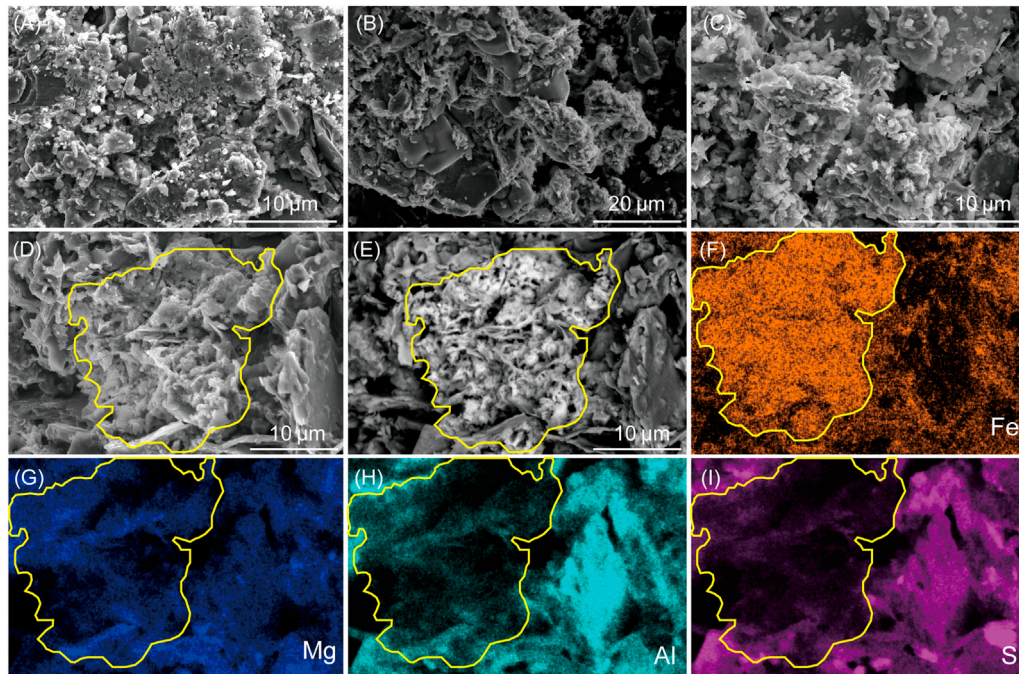


**FIGURE 5** | SEM micrographs of the clay minerals. **(A)** Clay morphology from sample 0718. **(B)** Clay morphology from sample 0719. **(C)** Clay morphology from sample 1222-3A. **(D)** Amorphous materials on the surface of clay grains. **(E)** Backscattered electron image of the amorphous materials. **(F)** Distribution of Fe in the same area as **(E)**. **(G)** Distribution of Mg in the same area as **(E)**. **(H)** Distribution of Al in the same area as **(E)**. **(I)** Distribution of Si in the same area as **(E)**.

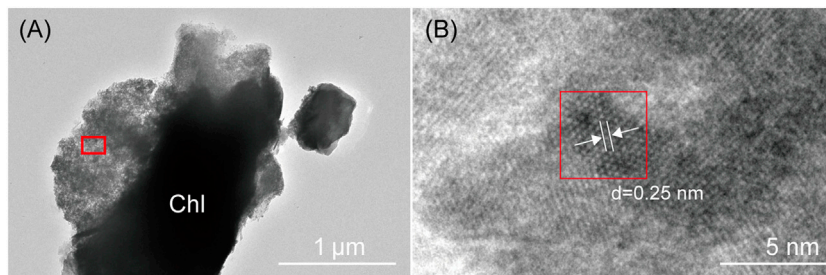


**FIGURE 6** | TEM micrographs of the rusty parts from 0718. **(A)** Fe-bearing materials associated with chlorite. **(B)** High-resolution TEM image of the Fe-bearing materials and the Fourier transform of a single crystal framed in the red rectangle.

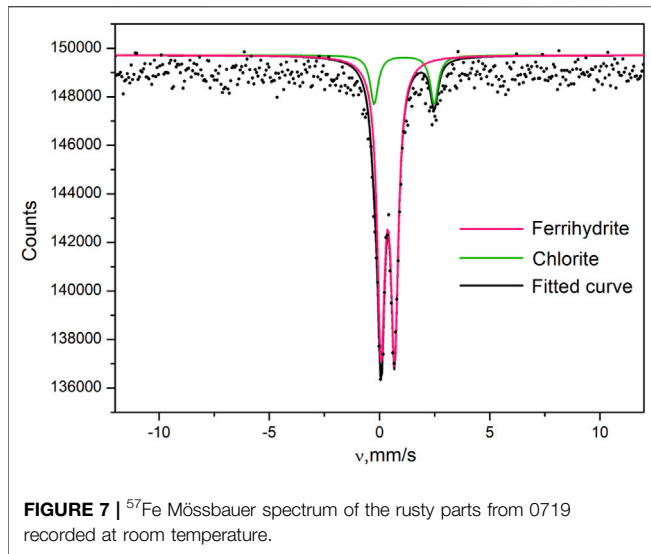
## DISCUSSION

### The Alteration of Clinocllore

As indicated by the XRD and EDS results, chlorite in the deposits was characterized as Fe-rich clinocllore because the chamosite has a different XRD pattern (Kohut and Warren, 2002). These minerals are detrital and sourced from the physical weathering of metamorphic and granitic parent rocks from the surrounding mountains (Miao et al., 2016). However, in the presence of post-depositional aqueous activity, the stability of clinocllore is affected. The deposits are loose and porous which provides intergranular space for the percolation of water. Previous experiments demonstrate that even in neutral to alkaline

fluids, chlorite can be partially altered to release iron to the aqueous repository (Malmström et al., 1996).

Along with the release of iron, the crystallinity of clinocllore decreases. Afterward, iron precipitates near the spots of weathering where the liquid water availability declines. The decreased intensity in XRD patterns and the reduction of Fe content determined by EDS provide both the structural and compositional evidence to support the above-proposed scenarios. Combined with the amorphous crystallinity and the Mössbauer hyperfine parameters, the post-weathering iron-bearing mineral was determined to be ferrihydrite. The SEM observations furnish the transformation of clay minerals with extra constraints as the content of Mg, Al, and Si decreases during the formation of amorphous ferrihydrite.



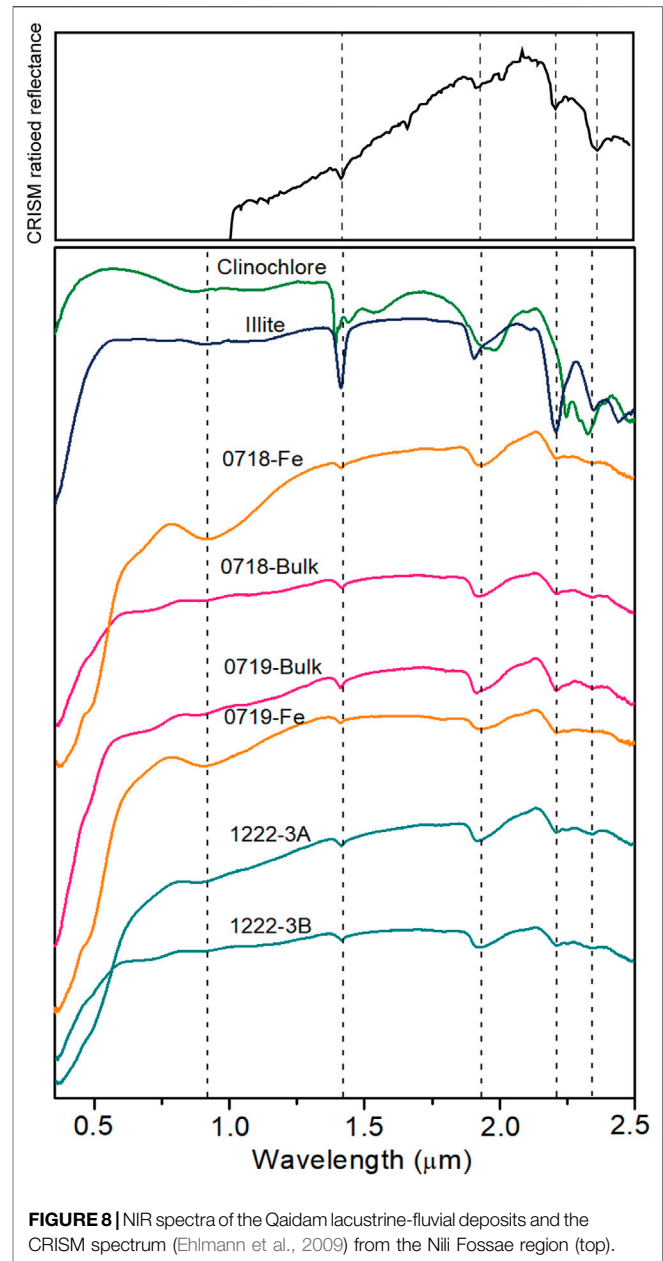
The clinocllore upon further weathering would be transformed to vermiculite and kaolinite associated with the evolution of Fe minerals from goethite to hematite in warm and wet conditions (Aspandiar and Eggleton, 2002a, b). However, as shown in **Figure 9**, the weathering reaction in the western Qaidam Basin is at the early stage which is hindered by the lack of liquid water in the prolonged hyperarid climate (Han et al., 2014). Rainwater or snowmelt can intermittently occur but be rapidly evaporated soon after the commencement of the weathering process. The low water availability may also be the reason that the weathering can only form amorphous iron hydroxides in the western Qaidam Basin.

Comparatively, illite is more stable than chlorite when exposed to post-depositional environments (Wilson, 1999). Considering the hyperarid climate in western Qaidam Basin, the alternation of illite is even negligible. Therefore, chlorite rather than illite is notably affected by post-depositional aqueous activity in the Qaidam deposits.

## Chlorite Illite Deposits on Mars

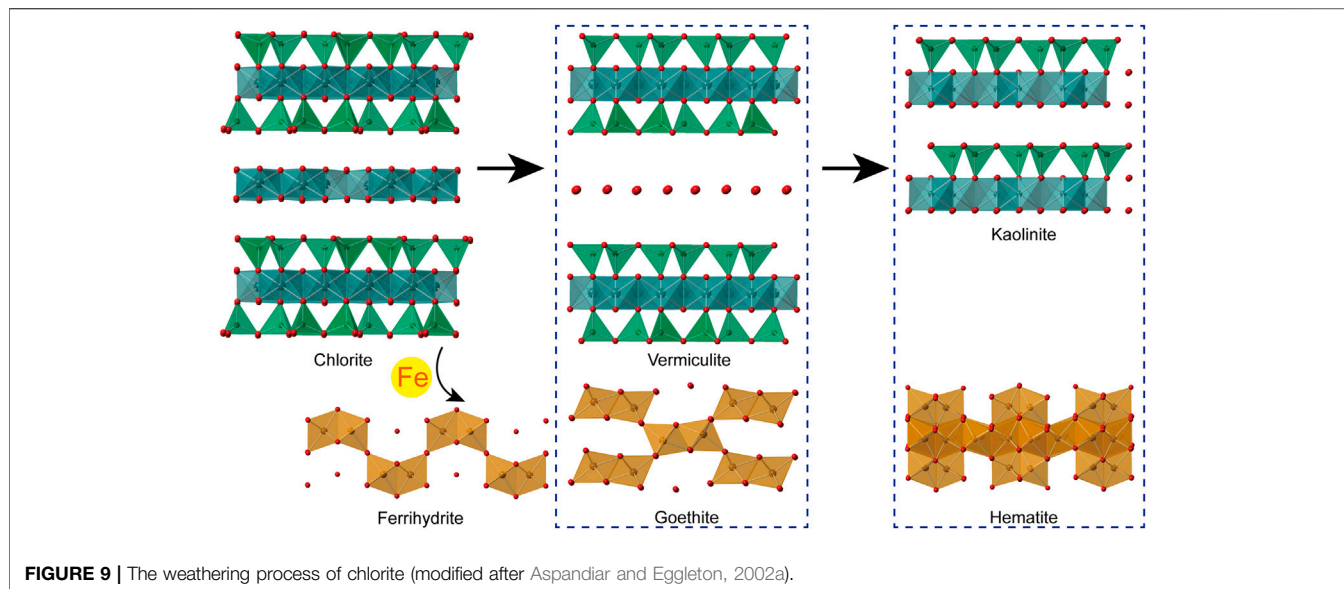
Martian chlorite illite deposits have previously been identified in Nili Fossae by NIR spectroscopy (**Figure 8**). In the region of Nili Fossae, alluvial activity shaped the stratigraphy of the area and left traces of large-scale flood events (Ehlmann et al., 2009; Mangold et al., 2007). The aqueous activity plays an important role in the mineralogy of these chlorite illite deposits because chlorite could be easily weathered to T-O-T clay minerals and iron hydroxide/oxides in the presence of liquid water (Aspandiar and Eggleton, 2002a, b). This process is essential to Martian deposits as liquid water might only be present occasionally for a long period through the geological time of Mars (Fairén, 2010; Bishop et al., 2018).

Cold and dry environments (e.g., permafrost areas, polar dry valleys, and the Qaidam Basin) where chlorite illite deposits distributed extensively are universally dominated by physical weathering (Bishop et al., 2008). Similar weathering processes



have likely existed on early Mars. By analyzing the rates of clay formation (Bishop et al., 2018), suggested that clay minerals on Mars could have formed in a relatively short geological time (tens of thousands of years), which is consistent with a more durable dry and cold climate model of early Mars (Mangold, 2021; Wordsworth et al., 2021).

On the Martian surface, chlorite is more common than illite due to the lack of  $\text{K}^+$  in most sedimentary remains (Ehlmann et al., 2009). (Ehlmann et al., 2011a) suggested that the Martian chlorite illite deposits were formed through diagenesis or subsurface low-grade metamorphism and were then transported by alluvial activities, which is comparable to the scenario in the western Qaidam Basin. Our results indicate



that subtle changes can still be happening with regional transient liquid activity. The most concentrated carbonate deposits on Mars are identified in the channel of Nili Fossae, which excludes the plausibility of extensive alteration from acidic fluids in this region (Ehlmann et al., 2009). Such situations and environments have dominated much of Martian history, which might leave possible aqueous information over minerals after the great change in global climate (McLennan et al., 2019).

The weathering process in Qaidam Basin is primarily driven by diagenesis, a process that might also play an important role in elemental migration on Mars. The abundance and mobility of Fe in the surface environment greatly affected the surface mineralogy of Mars (Tosca et al., 2008). The formation of widespread clay minerals is suggested to occur in the first billion years of Mars when the surface was aqueous and alkaline (Bibring et al., 2006; Ehlmann and Edwards, 2014). However, Fe can be released from clay materials easily to form nanophase hydroxides/oxides in the presence of limited liquid water. The post-depositional weathering process is likely still ongoing on the Martian surface, which could display a similar alteration tendency to the scenario in the Qaidam Basin. Although ferrihydrite is metastable in most terrestrial environments (Dehouck et al., 2017), evaluated the possibility of its presence on Mars by examining its transformation in varied conditions. The Mössbauer spectrographs acquired by the Spirit and Opportunity rovers and the XRD results from the CheMin onboard the Curiosity rover suggest the widespread occurrence of ferrihydrite (Rampe et al., 2016) or nanocrystalline hematite (Rampe et al., 2020) on Mars. Burial and heating of sediments would favor the transformation of these amorphous components into goethite and well-crystallized hematite; however, these scenarios might not occur after the weathering of Fe-clay

minerals in Martian sediments. Despite the neutral to alkaline conditions in Nili Fossae, acidity has evolved in most regions on Mars since the beginning of Hesperian (Zolotov and Mironenko, 2007), which can enhance the Fe-clay weathering and provide more sources for the widespread iron-bearing materials on Mars.

## CONCLUSION

Through the mineralogical study of chlorite illite deposits in the western Qaidam Basin, we observed the post-depositional effects on the change of chlorite composition and structure under hyperarid climatic conditions. Due to the ephemeral water activity, iron is released from Fe-clinochlore and forms amorphous ferric oxyhydroxides in the sediments. Similar NIR spectra are characterized in the Nili Fossae region on Mars, indicating the presence of chlorite illite deposits. Diagenesis in the Qaidam Basin and the resulting chemical weathering of chlorite may inform the evolution of chlorite and precipitation of secondary iron phases on the Martian surface.

## DATA AVAILABILITY STATEMENT

The datasets [ANALYZED] for this study can be found in the [Mendeley] <https://data.mendeley.com/datasets/xrrkt26zgt/1>.

## AUTHOR CONTRIBUTIONS

YS and YL planned this research. YS collected the samples and performed most experiments. CZ and XQ contributed to the analysis of XRD and NIR measurements. JS helped with the language. HH

and YP coordinated laboratory analyses and made constructive suggestions.

## FUNDING

This research was supported by NSFC (41621004 to YP), the CAS Strategic Priority Research Program (XDA17010501 to LT), and the National Natural Science Foundation of China (41921003). YL is funded by grants from the Research Grants Council of Hong Kong (RIF Project No: R5043-19).

## REFERENCES

- Aja, S., Omotoso, O., Bertoldi, C., Dachs, E., and Benisek, A. (2015). The Structure and Thermochemistry of Three Fe-Mg Chlorites. *Clays Clay Min.* 63 (5), 351–367. doi:10.1346/ccmn.2015.0630502
- Anglés, A., and Li, Y. (2017). The Western Qaidam Basin as a Potential Martian Environmental Analogue: An Overview. *J. Geophys. Res. Planets* 122 (5), 856–888. doi:10.1002/2017je005293
- Aspandiar, M. F., and Eggleton, R. A. (2002b). Weathering of Chlorite: II. Reactions and Products in Microsystems Controlled by Solution Avenues. *Clays Clay Min.* 50 (6), 699–709. doi:10.1346/000986002762090100
- Aspandiar, M. F., and Eggleton, R. A. (2002a). Weathering of Chlorite: I. Reactions and Products in Microsystems Controlled by the Primary Mineral. *Clays Clay Min.* 50 (6), 685–698. doi:10.1346/000986002762090227
- Bibring, J.-P., Langevin, Y., Mustard, J. F., Poulet, F., Arvidson, R., Gendrin, A., et al. (2006). Global Mineralogical and Aqueous Mars History Derived from OMEGA/Mars Express Data. *Science* 312, 5772400–5772404. doi:10.1126/science.1122659
- Bishop, J. L., Dobreá, E. Z. N., McKeown, N. K., Parente, M., Ehlmann, B. L., Michalski, J. R., et al. (2008). Phyllosilicate Diversity and Past Aqueous Activity Revealed at Mawrth Vallis, Mars. *Science* 321 (5890), 830–833. doi:10.1126/science.1159699
- Bishop, J. L., Fairén, A. G., Michalski, J. R., Gago-Duport, L., Baker, L. L., Velbel, M. A., et al. (2018). Surface Clay Formation during Short-Term Warmer and Wetter Conditions on a Largely Cold Ancient Mars. *Nat. Astron.* 2 (3), 206–213. doi:10.1038/s41550-017-0377-9
- Bishop, J. L. (2018). “Remote Detection of Phyllosilicates on Mars and Implications for Climate and Habitability,” in *From Habitability to Life on Mars* (Elsevier), 37–75. doi:10.1016/b978-0-12-809935-3.00003-7
- Cheng, F., Garzzone, C. N., Jolivet, M., Guo, Z., Zhang, D., Zhang, C., et al. (2019). Initial Deformation of the Northern Tibetan Plateau: Insights from Deposition of the Lulehe Formation in the Qaidam Basin. *Tectonics* 38 (2), 741–766. doi:10.1029/2018tc005214
- Dehouck, E., McLennan, S. M., Sklute, E. C., and Dyar, M. D. (2017). Stability and Fate of Ferrihydrite during Episodes of Water/rock Interactions on Early Mars: An Experimental Approach. *J. Geophys. Res. Planets* 122 (2), 358–382. doi:10.1002/2016je005222
- Ehlmann, B. L., and Edwards, C. S. (2014). Mineralogy of the Martian Surface. *Annu. Rev. Earth Planet. Sci.* 42, 291–315. doi:10.1146/annurev-earth-060313-055024
- Ehlmann, B. L., Mustard, J. F., Clark, R. N., Swayze, G. A., and Murchie, S. L. (2011a). Evidence for Low-Grade Metamorphism, Hydrothermal Alteration, and Diagenesis on Mars from Phyllosilicate Mineral Assemblages. *Clays Clay Min.* 59 (4), 359–377. doi:10.1346/ccmn.2011.0590402
- Ehlmann, B. L., Mustard, J. F., Murchie, S. L., Bibring, J.-P., Meunier, A., Fraeman, A. A., et al. (2011b). Subsurface Water and Clay Mineral Formation during the Early History of Mars. *Nature* 479, 737153–737160. doi:10.1038/nature10582
- Ehlmann, B. L., Mustard, J. F., Swayze, G. A., Clark, R. N., Bishop, J. L., Poulet, F., et al. (2009). Identification of Hydrated Silicate Minerals on Mars Using MRO-CRISM: Geologic Context Near Nili Fossae and Implications for Aqueous Alteration. *J. Geophys. Res.* 114, E2. doi:10.1029/2009je003339
- Fairén, A. G. (2010). A Cold and Wet Mars. *Icarus* 208 (1), 165–175. doi:10.1016/j.icarus.2010.01.006

## ACKNOWLEDGMENTS

We thank Dr. Xu Tang for his help with the TEM experiments.

## SUPPLEMENTARY MATERIAL

The Supplementary Material for this article can be found online at: <https://www.frontiersin.org/articles/10.3389/fspas.2022.875547/full#supplementary-material>

- Han, W., Fang, X., Ye, C., Teng, X., and Zhang, T. (2014). Tibet Forcing Quaternary Stepwise Enhancement of Westerly Jet and Central Asian Aridification: Carbonate Isotope Records from Deep Drilling in the Qaidam Salt Playa, NE Tibet. *Glob. Planet. Change* 116 (3), 68–75. doi:10.1016/j.gloplacha.2014.02.006
- Jiang, Z., Liu, Q., Roberts, A. P., Barrón, V., Torrent, J., and Zhang, Q. (2018). A New Model for Transformation of Ferrihydrite to Hematite in Soils and Sediments. *Geology* 46 (11), 987–990. doi:10.1130/g45386.1
- Kohut, C. K., and Warren, C. J. (2002). “Chlorites,” in *Chlorites: Soil Mineralogy with Environmental Applications* (Madison, WI: Soil Science Society of America, Inc.), 7, 531–553. doi:10.2136/sssabookser7.c17
- Kong, F., Zheng, M., Hu, B., Wang, A., Ma, N., and Sobron, P. (2018). Dalangtan Saline Playa in a Hyperarid Region on Tibet Plateau: I. Evolution and Environments. *Astrobiology* 18 (10), 1243–1253. doi:10.1089/ast.2018.1830
- Malmström, M., Banwart, S., Lewenhagen, J., Duro, L., and Bruno, J. (1996). The Dissolution of Biotite and Chlorite at 25 °C in the Near-Neutral pH Region. *J. Contam. Hydrol.* 21 (1-4), 201–213. doi:10.1016/0169-7722(95)00047-X
- Mangold, N. (2021). Intermittent Warmth on Young Mars. *Nat. Geosci.* 14 (3), 112–113. doi:10.1038/s41561-021-00700-9
- Mangold, N., Poulet, F., Mustard, J. F., Bibring, J.-P., Gondet, B., Langevin, Y., et al. (2007). Mineralogy of the Nili Fossae Region with OMEGA/Mars Express Data: 2. Aqueous Alteration of the Crust. *J. Geophys. Res.* 112, E8. doi:10.1029/2006JE002835
- McLennan, S. M., Grotzinger, J. P., Hurowitz, J. A., and Tosca, N. J. (2019). The Sedimentary Cycle on Early Mars. *Annu. Rev. Earth Planet. Sci.* 47, 91–118. doi:10.1146/annurev-earth-053018-060332
- Miao, W., Fan, Q., Wei, H., Zhang, X., and Ma, H. (2016). Clay Mineralogical and Geochemical Constraints on Late Pleistocene Weathering Processes of the Qaidam Basin, Northern Tibetan Plateau. *J. Asian Earth Sci.* 127, 267–280. doi:10.1016/j.jseas.2016.06.013
- Milliken, R. E., Swayze, G. A., Arvidson, R. E., Bishop, J. L., Clark, R. N., Ehlmann, B. L., et al. (2008). Opaline Silica in Young Deposits on Mars. *Geol.* 36 (11), 847–850. doi:10.1130/G24967A.1
- Murad, E. (1996). Magnetic Properties of Microcrystalline Iron (III) Oxides and Related Materials as Reflected in Their Mössbauer Spectra. *Phys. Chem. Miner.* 23 (4), 248–262. doi:10.1007/bf00207766
- Pollak, H., and Stevens, J. G. (1986). Phyllosilicates: A Mössbauer Evaluation. *Hyperfine Interact.* 29 (1), 1153–1156. doi:10.1007/bf02399439
- Poulet, F., Bibring, J.-P., Bibring, J.-P., Mustard, J. F., Gendrin, A., Mangold, N., et al. (2005). Phyllosilicates on Mars and Implications for Early Martian Climate. *Nature* 438, 7068623–7068627. doi:10.1038/nature04274
- Rampe, E. B., Bristow, T. F., Morris, R. V., Morrison, S. M., Achilles, C. N., Ming, D. W., Vaniman, D. T., Blake, D. F., Tu, V. M., Chipera, S. J., Yen, A. S., Peretyazhko, T. S., Downs, R. T., Hazen, R. M., Treiman, A. H., Grotzinger, J. P., Castle, N., Craig, P. I., Des Marais, D. J., Thorpe, M. T., Walroth, R. C., Downs, G. W., Fraeman, A. A., Siebach, K. L., Gellert, R., Lafuente, B., McAdam, A. C., Meslin, P. Y., Sutter, B., and Salvatore, M. R. (2020). Mineralogy of Vera Rubin Ridge from the Mars Science Laboratory CheMin Instrument. *J. Geophys. Res. Planets* 125 (9), e2019JE006306. doi:10.1029/2019je006306
- Rampe, E. B., Morris, R. V., Archer, P. D., Jr, Agresti, D. G., and Ming, D. W. (2016). Recognizing Sulfate and Phosphate Complexes Chemisorbed onto Nanophase

- Weathering Products on Mars Using *In-Situ* and Remote Observations. *Am. Mineralogist* 101 (3), 678–689. doi:10.2138/am-2016-5408CCBYNCND
- Ryan, P. C., and Reynolds, R. C. (1997). The Chemical Composition of Serpentine/chlorite in the Tuscaloosa Formation, United States Gulf Coast: EDX vs. XRD Determinations, Implications for Mineralogic Reactions and the Origin of Anatase. *Clays Clay Minerals* 45 (3), 339–352. doi:10.1346/ccmn.1997.0450305
- Smyth, J. R., Dyar, M. D., May, H. M., Bricker, O. P., and Acker, J. G. (1997). Crystal Structure Refinement and Mössbauer Spectroscopy of an Ordered, Triclinic Clinocllore. *Clays Clay Minerals* 45 (4), 544–550. doi:10.1346/ccmn.1997.0450406
- Sun, Y., Li, Y., Li, K., Li, L., and He, H. (2021). Massive Deposition of Carbonate Nodules in the Hyperarid Northwest Qaidam Basin of the Northern Tibetan Plateau. *Geochem Geophys Geosyst* 22, e2021GC009654. doi:10.1029/2021GC009654
- Sun, Y., Li, Y., Li, L., and He, H. (2019). Preservation of Cyanobacterial UVR-Shielding Pigment Scytonemin in Carbonate Ooids Formed in Pleistocene Salt Lakes in the Qaidam Basin, Tibetan Plateau. *Geophys. Res. Lett.* 46 (17–18), 10375–10383. doi:10.1029/2019gl083321
- Tosca, N. J., Knoll, A. H., and McLennan, S. M. (2008). Water Activity and the Challenge for Life on Early Mars. *Science* 320 (5880), 1204–1207. doi:10.1126/science.1155432
- Wilson, M. J. (1999). The Origin and Formation of Clay Minerals in Soils: Past, Present and Future Perspectives. *Clay Min.* 34 (1), 7–25. doi:10.1180/000985599545957
- Wordsworth, R., Knoll, A. H., Hurowitz, J., Baum, M., Ehlmann, B. L., Head, J. W., et al. (2021). A Coupled Model of Episodic Warming, Oxidation and Geochemical Transitions on Early Mars. *Nat. Geosci.* 14 (3), 127–132. doi:10.1038/s41561-021-00701-8
- Xiao, L., Wang, J., Dang, Y., Cheng, Z., Huang, T., Zhao, J., et al. (2017). A New Terrestrial Analogue Site for Mars Research: the Qaidam Basin, Tibetan Plateau (NW China). *Earth-Science Rev.* 164, 84–101. doi:10.1016/j.earscirev.2016.11.003
- Zolotov, M. Y., and Mironenko, M. V. (2007). Timing of Acid Weathering on Mars: A Kinetic-Thermodynamic Assessment. *J. Geophys. Res.* 112, E7. doi:10.1029/2006JE002882

**Conflict of Interest:** The authors declare that the research was conducted in the absence of any commercial or financial relationships that could be construed as a potential conflict of interest.

**Publisher's Note:** All claims expressed in this article are solely those of the authors and do not necessarily represent those of their affiliated organizations, or those of the publisher, the editors and the reviewers. Any product that may be evaluated in this article, or claim that may be made by its manufacturer, is not guaranteed or endorsed by the publisher.

Copyright © 2022 Sun, Li, Zhang, Qin, Shen, He and Pan. This is an open-access article distributed under the terms of the Creative Commons Attribution License (CC BY). The use, distribution or reproduction in other forums is permitted, provided the original author(s) and the copyright owner(s) are credited and that the original publication in this journal is cited, in accordance with accepted academic practice. No use, distribution or reproduction is permitted which does not comply with these terms.